3D-nHD: A HydroDynamic Model for Trap-Limited Conduction in a 3D Network

Andrea Cappelli, Rossella Brunetti and Carlo Jacoboni
Dept. of Physics, Mathematics and Computer Science,
University of Modena and Reggio Emilia
Italy
Email: andrea.cappelli@unimore.it

Enrico Piccinini
ARCES Research Center,
University of Bologna
Italy

Feng Xiong, Ashkan Behnam and Eric Pop
Dept. of Electrical and Computer Engineering
University of Illinois at Urbana-Champaign
Urbana, IL, USA

***Abstract*—Analytical models for trap-limited conduction have successfully been applied to the case of phase-change memory devices, providing an effective interpretation of the main charge-transport properties of chalcogenide materials. However they have been derived under the simplified hypothesis of one-dimensional continuum systems, and their extension to realistic geometries is anything but trivial. In this work we exploit a three-dimensional model for trap-limited conduction that makes use of a non-linear resistance network to implement the transport processes of the analytical models. Results correctly compare to experimental data and connect the transport properties to detailed microscopic information.**

I. Introduction

The largest part of today's non-volatile memory market is dominated by FLASH memories, either in the NAND or in the NOR configuration. According to the International Technology Roadmap for Semiconductors [1], this technology has already reached its maximum stage of development. Further enhancements aiming at increasing the storage capability and achieving substantial savings of the energy consumption are hampered by the intrinsic working principle of the floating gate [2].

Semiconductor industries have been considering alternative technologies in order to replace FLASH memories since at least ten years. Memory concepts where the information bit is encoded by means of a different resistance of the physical bit have been widely investigated. The resistance change of the memory bit can be obtained in several ways. The principal mechanisms are an electrically-activated phase change for the case of phase-change memories (PCM) [3], and the creation of highly-conductive filaments within a highly resistive matrix, as in oxide-based resistive memories (RRAM) [4] and in conductive-bridge memories (CBRAM) [5]. A similar behavior has also been observed in Ovonic materials [6], where the large resistivity change is introduced by a negative differential resistance. In general the Ovonic switch may be preliminary to a subsequent phase-change, so that PCM are manufactured with Ovonic materials like chalcogenides.

Phase-change memory prototypes where the metallic contacts of a "traditional mushroom" architecture (i.e., heater and top electrode) have been replaced with self-aligned carbon nanotubes allowed to obtain the smallest memory bit to date, with a strong prospective energy saving for next-generation PCM [7].

The knowledge of the microscopic mechanisms controlling conduction in switching chalcogenides is a key point in order to take an even better advantage from their properties. Many interpretations have been proposed in the literature (for a quick review see, e.g., Refs. [8] and [9]), and none of them is free from criticism. The trap-limited conduction scheme [10] gained a general consensus after the assessment of a thermally-activated transport mechanism until at least the threshold point [11]. The inclusion of the trap-limited framework in a hydrodynamic-like modeling approach confirmed that Ovonic threshold-switching is a purely electronic phenomenon connected to hot carriers [12].

Even though these models have been successfully applied to the case of PCM with a good fitting of experimental data, they have all been derived under the simplifying hypothesis of one-dimensional (1D) continuum systems. When the memory bit is shrunk down to few tens of nanometer or less, as in Refs. [7] and [13], these hypotheses may not apply any longer, and a more realistic three-dimensional (3D) description is needed. The 3D-nHD model used in this paper combines the concept of a three-dimensional resistance network to the hydrodynamic-like trap-limited transport model above for amorphous materials [14]. Once coupled to the Poisson equation, this scheme provides an effective and fast simulative framework that can easily be applied to realistic cell architectures including also non-conventional contacts.

II. The model

Numerical investigations on the atomic structure of chalcogenide materials showed that they feature a large number of defects [15]. As far as the transport properties are concerned, these defects act as scattering centers and dominate the conduction mechanism below threshold. We consider these centers as N randomly distributed nodes of a 3D network, whose connections exist when two nodes are closer than the cutoff distance r_{cut}. Two extra nodes (nodes 0 and $N+1$) placed at two opposite edges of the simulation domain play the role of the contacts, and cover the entire contact surfaces. The current I arriving at node 0 from the external circuit, or leaving node $N+1$ to the external circuit is prescribed.

978-1-4673-5736-4/13/$31.00 ©2013 IEEE

In order to write transport equations we conventionally label a current i_{ij} as incoming to node j from node i when $i < j$.[1] The Kirchoff's Current Law at the generic i-th node reads:

$$I\delta_{0,i}+\sum_{j<i} I_{ji} = \sum_{j>i} I_{ij}+I\delta_{i,N+1} \qquad i=0,\ldots,N+1. \quad (1)$$

Even though Eq. (1) allows one to write $N+2$ relationships, the set has rank $N+1$ as the current injected from the circuit at node 0 must be collected at node $N+1$ with no losses.

Currents I_{ij} can be expressed through proper transition rates T_{ij} that mimic trap-limited conduction between nodes i and j:

$$I_{ij} = -q(n_i T_{ij} - n_j T_{ji}), \quad (2)$$

where $-q$ is the charge of the electrons, and n_i the population sitting at the i-th node. Inserting Eq. (2) in Eq. (1) yields the charge-flux balance:

$$\frac{I}{(-q)}\delta_{0,i} + \sum_{j\neq i} n_j T_{ji} = \sum_{j\neq i} n_i T_{ij} + \frac{I}{(-q)}\delta_{i,N+1}. \quad (3)$$

In order to estimate the transition rate T_{ij} in the present model, one has to recall the basic ideas of trap limited conduction:

1) a number n_i of carriers populate the node i of the network. While sitting at a node, carriers belong to a localized state with energy e_i;
2) a three-stage mechanism is responsible for carrier transfer: carrier emission to a traveling state above the conduction band mobility edge E_C, propagation in the traveling state towards another node and recapture by the final node with a probability $f(r_{ij})$, depending on the internode distance r_{ij};
3) the local field F_{ij} alters the height of the energy barrier a carrier must overcome to be emitted, enhancing the motion in one direction and hindering it in the opposite direction. The energy barrier is evaluated after an effective distance ℓ from the emitting site [16];
4) carriers can gain energy from the field and release energy to the lattice via phonon scattering.

The following transition rate encompasses the properties above and has been adopted in the 3D-nHD model:

$$T_{ij} = \frac{f\,(r_{ij})}{\tau_0} \exp\left(-\frac{E_C - e_i}{k_B T_L}\right) \exp\left[\frac{-q(\varphi_i-\varphi_j)\ell}{r_{ij}\,k_B T_L}\right], \quad (4)$$

where τ_0, k_B, and T_L are a characteristic time of the transfer process, the Boltzmann constant and the lattice temperature, respectively. The local field is estimated by means of its first-order approximation $F_{ij} = (\varphi_j - \varphi_i)/r_{ij}$, with φ_i and φ_j the electrostatic potentials of the i-th and j-th nodes. For simplicity, we have assumed $f(r_{ij})$ the step function within the cutoff distance r_{cut}.

Point 4) above allows one to write also energy flux equations, that define the steady-state value of the energy of the carriers sitting at a given internal node. Since nodes 0 and $N+1$ represent the contacts, their population and energy is fixed at the equilibrium values. Similarly to Eq. (3), in order to derive the energy flux equations, one has to balance the incoming energy gains at a given node i from the other nodes j of the network, modulated by the local field, to the energy losses of the outgoing carriers and due to the energy relaxation with the lattice:

$$\begin{aligned}\sum_{j\neq i} n_j T_{ji}\Big[e_j - q(\varphi_j-\varphi_i)\Big] + \frac{I}{(-q)}e_i\delta_{0,i} = \\ = e_i\Big[\sum_{j\neq i} n_i T_{ij} + \frac{I}{(-q)}\delta_{i,N+1}\Big] + n_i\frac{e_i - e_{i,eq}}{\tau_R},\end{aligned} \quad (5)$$

with τ_R the energy-relaxation time constant and $e_{i,eq}$ the energy of a carrier at the i-th node under equilibrium conditions.

The solution of Eqs. (3) and (5) requires particular care due to the strong non linearities of the equation terms as functions of the unknowns φ_i and e_i. Moreover, in order to achieve self-consistency between the nodal population n_i and the electrostatic potential φ_i, the Poisson equation must be invoked. A multi-step iterative procedure has been implemented. At first, Eqs. (3) and (5) are mutually solved for a prescribed current I and for a fixed nodal population n_i, yielding the electrostatic potentials on the network φ_i and the carrier energies n_i. This step has been tackled by means of a Newton-Raphson (NR) algorithm by which half of the unknowns are alternatively kept fixed or updated. Once the solution has converged, a finite-element (FEM) procedure is implemented to calculate the carrier concentrations from the Poisson equation, using the previously determined electrostatic potentials as Dirichlet conditions. The finite-element grid involves of a large number of nodes, part of which coincides with the transport network nodes. The NR-FEM algorithm is cycled until global convergence is achieved, which is usually obtained within few iterations.

III. Results

A. Stochastic analysis of the current vs. voltage characteristics

Experimentally, fluctuations of two kinds are found for the measured voltage V at a given input current I. Large fluctuations occurring in the first fires (*burn-in* or *forming* process) [13] can be associated with the changes in the structure of the amorphous matrix, initially created via sputtering and next modified with crystallization/re-amorphization cycles via Joule heating. These fluctuations progressively reduce and after few tens of cycles they disappear. Then, only smaller fluctuations are found. The latter can be explained by considering the positions of the defects inside the amorphous matrix, that slightly change at each crystallization/re-amorphization cycle.

These fluctuations can be simulated with the 3D-nHD model: in order to check the I–V characteristics predicted by the 3D-nHD model against experimental evidences, batches of samples differing only in the positions of the network nodes must be taken into account, and the variance of the results can be estimated. In Fig. 1 we report the average I–V characteristic from 50 samples along with the corresponding standard deviation. Results are compared to recent experimental data obtained for memory concepts with carbon-nanotube electrodes, which represent an ultra-scaled prototype of a memory bit ($\sim$ 10nm

[1] This notation is just mathematical, without any connection with the effective sign of the current, which can be either positive or negative (reversing the concepts of incoming or outgoing current).

in diameter) [13]. The abrupt voltage drop at $I \sim 350$ nA indicates that crystallization of the sample occurred, which is not addressed by this version of the model. The good agreement of the I–V characteristics in the sub-threshold regime and up to the threshold point (i.e., $\mathrm{d}V/\mathrm{d}I \approx 0$) let us extract the model parameters that are listed in the caption.

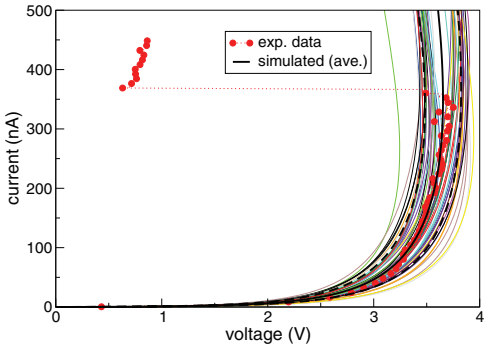

Fig. 1. Statistical analysis of the current vs. voltage characteristics of a memory prototype with carbon nanotube contacts (estimated size: $10 \times 10 \times 40$ nm^3) compared to experimental evidences [13]. The marked solid line is the average value of 50 samples; the two dashed side lines indicate the upper and lower limits determined by the standard deviation σ. Parameters used for fitting: $\tau_0 = 49.5$ fs, $\tau_r = 56$ fs, $\ell = 2.9$ nm, $E_C = 0.3$ eV, $r_{cut} = 6$ nm, node concentration 1.2×10^{-19} cm^{-3}.

We notice that the 3D-nHD model is rather sensitive to the interaction distance r_{cut}; Fig. 2 shows the dispersion of the calculated threshold point for progressively increasing values of r_{cut} in the range 6-9 nm. Longer interaction distances lead to narrower distributions for the threshold voltage and to larger distributions for the threshold current, as shown by the rectangles that indicate the standard deviations of the four distributions. As the interaction distance lengthen, the approximation of the capture probability $f(r_{ij})$ given in the previous section may need to be improved to limit the contribution of the longest transition, that are unlikely to happen in amorphous materials. From these results, we claim r_{cut} a critical parameter in order to give predictive estimates of a device behavior. At present, in the lack of any quantitative information from first-principle transport calculations, its value should be determined from the comparison of the simulated results to an extensive experimental investigation.

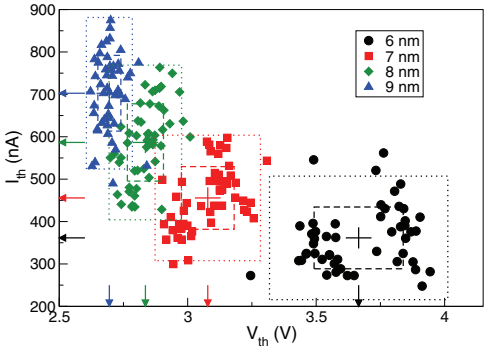

Fig. 2. Variability of the position of the switching point (V_{th}, I_{th}) for the test device of Fig. 1 as a function of the interaction distance r_{cut}. The average values of the threshold voltage and currents are indicated by the crosses and by the arrows pointing to the axes. The dashed and the dotted rectangles enclose points differing from the average value less than one or two σ's, respectively.

B. *Preferential paths for conduction*

Apart from the fluctuations described in previuos paragraph, all of the I–V characteristics share the typical pattern of the hot-carrier trap-limited conduction outlined by the 1D models. Specifically, we observe the presence of three different conduction regimes (Ohmic, exponential, and super-exponential) in the I–V characteristic up to the threshold condition, and the negative-differential-resistance (NDR) condition sets in after threshold. According to the models in the literature, this behavior can be ascribed either to the presence of hot carriers, or to the formation of preferential paths leading to filamentary conduction. In particular, 1D models [12], [17] can neither confirm nor invalidate the existence of preferential paths. On the other hand, filamentary conduction was highlighted by other models using an electro-thermodynamical approach [18], without detailing the transport mechanisms at the nanoscale. The 3D-nHD model allows to track highly-conductive paths related to carrier heating.

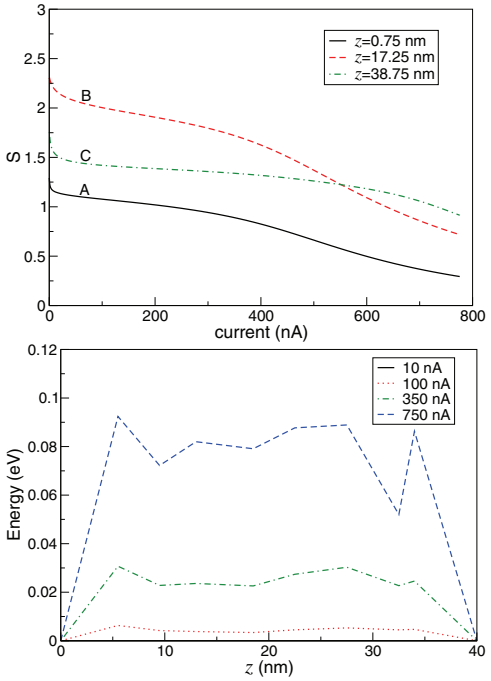

Fig. 3. Top panel: Concentration of the current along preferential path as a function of the prescribed current for the three sections indicated in Fig. 4. The monotonically decreasing behavior indicates that the current is progressively gathered by a single path per section (see text). Bottom panel: Specific energy of the nodes along the preferential path, as a function of the z coordinate. Four currents, one per conduction regime, are reported. The energy of the two contacts is prescribed at the equilibrium value $e_{eq} = 0$.

The microscopic details of the conduction mechanism connected to the creation of a preferential path of hot carriers are shown in Fig. 3. To this aim, we use the function $S(z) = -\sum_{i,j} \theta_{ij}(z) \ln[\theta_{ij}(z)]$, where $\theta_{ij}(z) = I_{ij}(z)/I$ is the fraction of the prescribed current I flowing between pairs of nodes i and j (with $i < j$) placed at opposite sides of a cross-section at a given z coordinate [19]. Such a function estimates the degree of disorder over a cross-section of the network. In the top panel of Fig. 3 we report the values calculated on three sections, two near the two contacts (A and C) and one in the middle of the device (B). The high initial values means that the current is almost evenly distributed over

all paths crossing the section and the differences are basically due to the different numbers of lines that must be counted in the three cases. The progressive significant decrease of the entropy for sections A and B indicates that the charge flux concentrates along a particular path, gathering the majority of the current. This behavior is present also for section C, though less pronounced, since in this case a preferred path dominates over its competitors even at low currents.

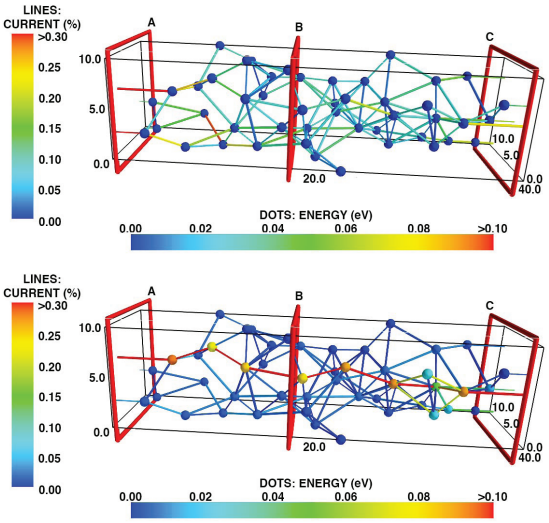

Fig. 4. 3D representation of the network and creation of the preferential conductive path. The two images refer to a very low current (top) and to a high current after threshold switching (bottom). The positions of sections A, B, and C used in Fig. 3 are also shown.

The presence of hot carriers is revealed by analyzing the specific energy e_i of the nodes of the preferential path. In the bottom panel of Fig. 3 we report the specific energy profile as a function of the distance from the injecting contact at $z = 0$ for four selected values of the current. In pre-switching conditions, the imbalance between energy gain and relaxation activates some nodes with a substantial increase in the specific energy of the carriers sitting there. Since the transition rates have a strong dependence on such an energy, this hot-carrier effect triggers a positive feedback that reinforces the current along the preferential path, and a low-resistance, contact-to-contact route is eventually created. As a consequence, the voltage dropped across the device is reduced when the current is further increased. The microscopic configurations of the network for a low current far from threshold and a high current after threshold are also represented in the two ball-and-stick plots of Fig. 4.

IV. Conclusion

A 3D extension of the hydrodynamic-like model for trap-limited conduction in amorphous materials has been derived and implemented within the framework of a non-linear resistance network. The outcomes of the simulations fit nicely the test case of PCM prototypes, and provide information about the statistical variability of the threshold condition. A sound microscopic interpretation based on preferential paths of hot carriers is also provided. A future extension of the 3D-nHD model will also take into account lattice heat transport and crystallization effects.

Acknowledgment

The Italian authors acknowledge financial support from the Intel Corp. through grant No. 3477131/2011. The Illinois authors acknowledge support from the U.S. Office of Naval Research (grant N00014-10-1-0853) and the U.S. National Science Foundation (grant ECCS 1002026).

References

[1] *The International Technology Roadmap for Semiconductors: 2012 update.*

[2] Derhacobian N., Hollmer S.C., Gilbert N., and Kozicki M.N., "Power and energy perspective of nonvolatile memory techonologies", *Proc. IEEE*, **98**, 283 (2010).

[3] Wong H.-S.P., Raoux S., SangBum K., Jiale L., Reifenberg, J.P., Rajendran B., Asheghi M., and Goodson K.E., "Phase Change Memory", *Proc. IEEE*, **98**, 2201 (2010).

[4] Wong H.-S.P., Lee H.-Y., Yu S., Chen Y.-S. Wu, Y., Chen, P.S., Lee B., Chen, F.T., and Tsai M.-J., "Metal-oxide RRAM", *Proc IEEE*, **100**, 1951 (2012).

[5] Kozicki, M.N., and Mira Park Mitkova M., "Naoscale memory elements based on solid-state electrolytes", *IEEE Trans. Nanotechnol.*, **4** 331 (2006).

[6] Ovshinsky S.R, "Reversible electrical switching phenomena in disordered structures", Phys. Rev. Lett., **21**, 1450 (1968).

[7] Xiong F., Liao A.D., Estrada D., and Pop E., "Low-power switching of phase-change materials with carbon nanotube electrodes", *Science*, **332**, 568 (2011).

[8] Jacoboni C., Piccinini E., Buscemi F., and Cappelli A., "Hot-electron conduction in ovonic materials", *Solid-State Electron.*, **84**, 90 (2013).

[9] Nardone M., Simon M., Karpov I.V., and Karpov V.G., "Electrical conduction in chalcogenide glasses of phase change memory", *J. Appl. Phys.*, **112**, 071101 (2012).

[10] Ielmini D., and Zhang Y., "Analytical model for subthreshold conduction and threshold switching in chalcogenide-based memory devices", *J. Appl. Phys.*, **102**, 054517 (2007).

[11] Ielmini D., and Zhang Y., "Evidence for trap-limited transport in the subthreshold conduction regime of chalcogenide glasses", *Appl. Phys. Lett.*, **90**, 192102 (2007).

[12] Piccinini E., Cappelli A., Buscemi F., Brunetti R., Ielmini D., Rudan M., and Jacoboni C., "Hot-carrier trap-limited transport in switching chalcogenides", *J. Appl. Phys.*, **112**, 083722 (2012).

[13] Xiong F., Bae, M.-H., Dai Y., Liao A.D., Behnam A., Carrion E.A., Hong S., Ielmini D., and Pop E., "Self-aligned nanotube/nanowire phase change memory", *Nano Lett.*, **13**, 464 (2013).

[14] Cappelli A., Piccinini E., Xiong F., Behnam, A., Brunetti R., Rudan M., Pop E., and Jacoboni C, submitted for publication (2013).

[15] Caravati S., Bernasconi M., Kühne, T.D., Krack M., and Parrinello M., "First-principles study of crystalline and amorphous $Ge_2Sb_2Te_5$ and the effects of stoichiometric defects", *J. Phys: Condens. Matt.*, **22**, 205502 (2010).

[16] Betti Beneventi G., Guarino L., Ferro M., and Fantini P., "Three-dimensional Poole-Frenkel analytical model for carrier transport in amorphous chalcogenides", *J. Appl. Phys.*, **113**, 044506 (2013).

[17] Ielmini D., "Threshold switching mechanism by high-field energy gain in the hopping transport of chalcogenide glasses", *Phys. Rev. B*, **78**, 035308 (2008).

[18] Simon M., Nardone M., Karpov I.V., and Karpov V.G., "Conductive path formation in glasses of phase change memory", *J. Appl. Phys.*, **108**, 064514 (2010).

[19] Pershin Y.V., and Di Ventra M., "Self-organization and solution of shortest-path optimization problems with memristive networks", http://arxiv.org/abs/1304.1675v1 (2013).